HAL open science

Lattice Boltzmann simulation of advection-diffusion of chemicals and applications to blood flow

Hengdi Zhang, Chaouqi Misbah

▶ **To cite this version:**

Hengdi Zhang, Chaouqi Misbah. Lattice Boltzmann simulation of advection-diffusion of chemicals and applications to blood flow. Computers and Fluids, 2019, 187, pp.46-59. 10.1016/j.compfluid.2019.04.018 . hal-02397342

HAL Id: hal-02397342

https://hal.science/hal-02397342v1

Submitted on 22 Oct 2021

HAL is a multi-disciplinary open access archive for the deposit and dissemination of scientific research documents, whether they are published or not. The documents may come from teaching and research institutions in France or abroad, or from public or private research centers.

L'archive ouverte pluridisciplinaire **HAL**, est destinée au dépôt et à la diffusion de documents scientifiques de niveau recherche, publiés ou non, émanant des établissements d'enseignement et de recherche français ou étrangers, des laboratoires publics ou privés.

Distributed under a Creative Commons Attribution - NonCommercial 4.0 International License

Version of Record: https://www.sciencedirect.com/science/article/pii/S004579301930132X
Manuscript_bc84abd737b9cd6c5472f10af353c182

Lattice Boltzmann Simulation of Advection-Diffusion of Chemicals and Applications to Blood Flow

Hengdi Zhang, Chaouqi Misbah*

Univ. Grenoble Alpes, CNRS, LIPhy, 38000 Grenoble, France

Abstract

Diffusion of solutes is often encountered in many biological processes. In the blood micro circulation system, solutes, such as oxygen and calcium molecules, as well as Adenosine Triphosphate (ATP) and biochemical messengers, are released by cells (like red blood and endothelial cells), and are dispersed via diffusion and advection. Moreover, several targeted drug delivery strategies rely on an encapsulation of chemicals and on their release in the blood stream at specific location. The released chemicals couple to blood flow, in which red blood cells (RBCs) constitute the major component. Thus, the development of numerical methods which take into account both dynamics of RBCs and their coupling with chemicals is of great importance for many biomedical applications. We develop here a lattice-Boltzmann based method that deals with generic moving boundary conditions in an advection-diffusion field representing the chemicals. The boundary condition of the solutes at the cell membrane is based on a modified bounce-back scheme. We prove analytically, and validate numerically, that it enjoys second order precision. The solver is validated with

*Corresponding author
Email address: chaouqi.misbah@univ-grenoble-alpes.fr (Chaouqi Misbah)

© 2019 published by Elsevier. This manuscript is made available under the CC BY NC user license
https://creativecommons.org/licenses/by-nc/4.0/

several benchmarks and is then coupled with a solver for a suspension of RBCs, we developed previously. We then exemplify the method on the problem of liposome drug delivery in arterioles. The results show that for a rigid drug carrier at a scale of about 1 μm, the presence of RBCs facilitates the drug absorption along the vessel wall. We also exemplify the solver for the release of chemicals induced by membrane shear stress, a feature which is omnipresent in mechano-involved signaling processes. As a way of example, we briefly study the problem of ATP release by RBCs. We point out several possible generalizations.
Keywords: lattice boltzmann, blood flow, chemical signaling

1. Introduction

In many biological processes cytoplasmic membranes play an important role regarding molecular and ion (active and passive) transport from the cell interior towards the extra cellular environment and vice versa. Examples are abundant in blood circulation. For instance, red blood cells (RBCs) can release oxygen as well as ATP in the microcirculation zone depending, in particular, on the oxygen pressure as well as on the cell membrane shear stress Forsyth et al. (2011); Zhang et al. (2018). Other examples are encountered in endothelial signaling pathways modulating vasodilation Davies (1995); Yamamoto et al. (2000); Ando and Yamamoto (2013), or in the lymphatic system where calcium dynamics plays a decisive roleZawieja (2005); Jafarnejad et al. (2015). Solute transport is also an active field of research in biotechnologies, such as targeted drug delivery which relies on an encapsulation of chemicals within liposomes which are then released at specific sites; the release is triggered either by intrin-

sic properties (e.g. local shear stress) or by means of an external stimulus (e.g. ultrasound) Needham et al. (2000); Allen and Cullis (2013); Akbarzadeh et al. (2013); Sercombe et al. (2015); Kaoui (2018). All these examples involve an intimate coupling between blood flow and chemical transport. In other words, the chemical species, besides reactions and diffusion, are advected by the flow. In addition, the chemical species are bound within moving and deformable domains (e.g. RBCs, drug carriers, such as liposomes, etc.). RBCs constitute the major obstacle against solute dispersion in the blood stream. We have thus to cope the coupling between the moving boundaries, the flow field and chemical transport with specific boundary conditions on the membranes of the suspended entities (e.g. liposomes, RBCs) describing the condition under which the solute is released. This task is, in its full generality, quite complex and presents several numerical and conceptual challenges to be described below.

The main purpose of this paper is to develop an advection-diffusion method in the presence of deformable particles (like RBCs or liposomes). This problem will be formulated and solved by means of a lattice Boltzmann method (LBM). The solution of the pure fluid flow by LBM has now become quite classical Zou and He (1997); He and Luo (1997); Chen and Doolen (1998); Succi (2001); Mohamad (2011); Krüger et al. (2013); Krüger et al. (2017). The diffusion/advection problem is now becoming an emerging field of research from both physical and numerical aspects Mohamad (2011); Krüger et al. (2017); Huang et al. (2009); Lee et al. (2010); Markl and Körner (2015); Chen et al. (2013a); Zu and He (2013); Fakhari et al. (2017); Liu et al. (2018). To the best

of our knowledge, a LBM with general moving boundary with Dirichlet (the boundary concentration is specified) / Neumann (the normal derivative is specified) / Robin (a linear combination of boundary concentration and its normal derivative is specified) condition has not been addressed yet.

We will develop here a LBM for the diffusion-advection problem and couple it with the fluid solver. The formulation of the coupling of the fluid flow to the chemicals adds an extra layer of complexity. A formidable task is to properly handle the chemical boundary conditions on a curved and moving interface (the cell membrane). We will see that both the curvature as well as the moving boundary character pose a challenge. The difficulty arises from the fact that the chemical concentration can be discontinuous at the boundary, unlike the velocity field which is continuous and where the so-called immersed boundary method (IBM) has been successfully applied. Except for some specific situations (the diffusion profile is smooth; the profile has a finite thickness across the membrane) Peskin (2002); Feng and Michaelides (2004); Yang et al. (2009); Huang et al. (2009); Lee et al. (2010,?); Chen and Lai (2014), the use of IBM for general problems remains to be shown. **Another alternative than LBM for treating diffusion has been dealt with recently Liu et al. (2018). In that work a combination of a Langevin equation (for nanoparticles) and LBM (for RBCs) is adopted. When chemical reactions are present, as well as when general boundary conditions are prescribed at the moving boundaries, a generalization of this spirit remains to**

be done.

A generic type of boundary conditions at the membrane that we will deal with is the so-called Robin boundary condition. This question has been addressed for a static curved boundaryGebäck and Heintz (2014); Zhang et al. (2012); Chen et al. (2013b); Li et al. (2013); Huang et al. (2016). This problem was addressed in a way which requires an interpolation strategy and local curvature information, making its parallel implementation for arbitrary moving curved boundaries challenging. Huang et al.Huang and Yong (2015) proposed another simplified scheme for general Robin condition on piecewisely linear segments (which are parallel to the mesh segment) with second order precision. The formulation of the boundary condition is derived via asymptotic analysis Junk et al. (2005); Yoshida and Nagaoka (2010), and requires only local information. Later on Huang et al. (2016) an extension of this scheme for curved boundaries with second order precision has been proposed. However, this scheme turned out to present an interpolation strategy which is shape-dependent and requires information on the local curvature.

In order to circumvent the problem of inefficiency for parallel implementation and challenges raised by some specific shapes, we have developed, by still adopting the general Robin boundary condition scheme from Huang and Yong (2015), a simplified interpolation scheme. Indeed, our scheme takes into account only a single neighboring lattice point to the membrane, instead of several lattice points Huang et al. (2016). It will be shown here that the simplified version still enjoys the same precision, but at the same time it offers the possibility

of efficient (parallel efficiency) and robust handling of arbitrary and moving boundaries.

In addition to the above complexity due to boundary shape, the motion of the boundary in itself raises another problem. Indeed, in the course of time lattice points belonging to a domain lying on one side of the membrane may shift to the other side, and vice versa. Thus, we must identify at each time step the points which have been swept by the moving boundary. This requires an interpolation and / or extrapolation scheme in order to properly reset the values of the concentration field (in the classical fluid-structure interaction problem , this is the so-called refilling procedure Lallemand and Luo (2003)). Our method uses a similar spirit as the refilling procedure, but introduces some improvement, as will be described here.

Due to the general complexity of the problem we will focus here on a 2D geometry. The implementation of the chemical problem in LBM is based on the so-called D2Q5-BGK model (2 dimensional, 5 velocity and Bhatnagar-Gross-Krook single relaxation time). To efficiently exploit the parallelization benefit of LBM, the implementation is fully based on a graphic processing unit (GPU) parallel architecture, namely Compute Unified Device Architecture (CUDA). Several tests are performed in order to demonstrate the precision and validity under static and moving boundary conditions.

After having performed several convergence and validation tests, we integrate this solver into a well-validated immersed-boundary coupled Navier-Stokes LBM solver Shen et al. (2017). We then present two main applications: (i)

we study the liposome drug delivery (caused by an external stimulus) problem and analyze the main outcome. Particularly important contributions have been made by Kaoui Kaoui (2018) and others Kabacaoğlu et al. (2017) who analyzed the problem of drug release and solute mixing. Another impotant study has analyzed advection-diffusion under steady flow for a given shape (a cylinder) Gekle (2017). Here we extend these studies to the case where the suspended entities (e.g. model of RBCs) are both deformable (free moving boundaries) and coupled to the advection-diffusion of the solute. (ii) We shall adapt the method to the case where the membrane boundary condition depends on the local shear stress, with the aim to analyze mechano-involved signaling process in micro-circulation. Of particular interest is the problem of ATP release from RBCs that will be briefly presented.

2. Methods

Since the problem of solving the Navier-Stokes equations by LBM has by now become quite classical Zou and He (1997); He and Luo (1997); Chen and Doolen (1998); Succi (2001); Mohamad (2011); Krüger et al. (2017), we will focus on the convection-diffusion problem, and only briefly recall the LBM for the fluid when needed. The proposed method can handle several solutes which are coupled to each other. However, for ease of presentation we will consider a single solute only. In addition, we will restrict ourselves to a two dimensional domain (denoted as 2D), and thus our model of RBC will be a 2D contour made of an inextensible membrane. **It will be recognized that a generalization**

to many solutes is straightforward. Let c denote the concentration of a given solute that depends on space and time. In its full generality c obeys the following equation

$$\frac{\partial c}{\partial t} + \mathbf{u} \cdot \nabla c = \nabla \cdot [D(t, \mathbf{x}) \nabla c] + R(c, t, \mathbf{x}) \tag{1}$$

$\mathbf{u}$ is the velocity field (supposed to be known for the moment), $t \in \mathbb{R}^+$ and $\mathbf{x} \in \mathbb{R}^2$ are time and spatial coordinates, respectively. For simplicity, we assume here that the diffusion coefficient D is constant. The reaction term R can be handled within the LBM method (in the same way as an external force in the usual fluid solver). A non-overlapping moving boundary (say a RBC model in 2D) curve is explicitly defined as $\mathbf{B}(t, s) = [X(t, s), Y(t, s)]$, here X and Y are Cartesian components of a given membrane point, s is a scalar parameter, which can typically be chosen as the local arc length. By adopting for the fluid flow the non-slip condition assumption at the membrane, the boundary is advanced by the adjacent fluid velocity

$$\frac{\partial \mathbf{B}}{\partial t} = \mathbf{u}(t, \mathbf{B}) \tag{2}$$

If s is chosen as the local arc-length, the normal vector of the boundary is defined as $\mathbf{n}(t, s) = [-\partial Y/\partial s, \partial X/\partial s]$, while tangential vector is defined as $\mathbf{t}(t, s) = [-\partial X/\partial s, -\partial Y/\partial s]$

The solute concentration c and the corresponding flux $\mathbf{J} = \mathbf{u}c - D\nabla c$ are, in general, discontinuous at the boundary. By defining $c^{\pm}(\mathbf{B}) = \lim_{\epsilon \to 0^{\pm}} c(\mathbf{B} + \epsilon \mathbf{n})$, ($c^{\pm}$ in short), the general Robin boundary condition (an equation which

combines both Neumann and Dirichlet conditions) along the two sides of the moving boundary $\mathbf{B}$ can be written as

$$\begin{cases} \alpha_1^+ c^+ + \alpha_2^+ \mathbf{n} \cdot \nabla c^+ = \alpha_3^+ \\ \alpha_1^- c^- + \alpha_2^- \mathbf{n} \cdot \nabla c^- = \alpha_3^- \end{cases} \tag{3}$$

Here α_i's are real constant. A schematic of the moving boundary and some definitions are shown in Fig. 1a.

2.1. Advection-Diffusion Lattice Boltzmann Method

We adopt the so-called D2Q5 BGK model (2 dimensional 5 velocities and a single relaxation time) to formulate a convection-diffusion lattice Boltzmann scheme. Compared to the classical D2Q9 models (used for the fluid solver Zou and He (1997); He and Luo (1997); Chen and Doolen (1998); Succi (2001)), D2Q5 requires a smaller memory usage and lends itself to an easier treatment for the geometry of the moving boundary, both of which are important for acceleration in a GPU parallel context. In addition, there are numerical evidences that D2Q5 may enjoy a better stability against D2Q9 for the diffusion problem in some particular situations such as at low or intermediate Peclet numbers Li et al. (2017); Suga (2006).

Let Δx and Δt denote the spatial and temporal mesh sizes, the discrete micro velocities are defined as

$$\begin{bmatrix} \mathbf{c}_0 & \mathbf{c}_1 & \mathbf{c}_2 & \mathbf{c}_3 & \mathbf{c}_4 \end{bmatrix} = \begin{bmatrix} 0 & 1 & -1 & 0 & 0 \\ 0 & 0 & 0 & 1 & -1 \end{bmatrix} \frac{\Delta x}{\Delta t} \tag{4}$$

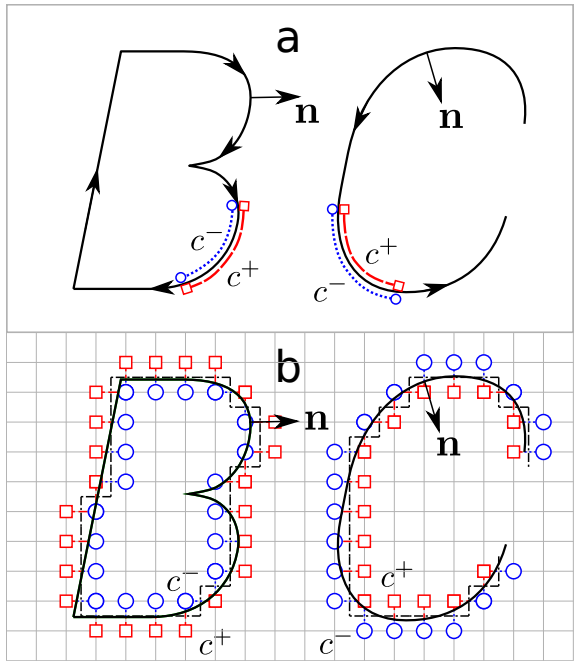

Figure 1: A schematic of the convection-diffusion problem in the presence of a moving boundary: a) physical boundary $\mathbf{B}(t, s)$ is piecewisely continuous with countable discontinuities in its derivative. Boundary conditions expressed by Eq. (3) are imposed along each side of the curve. Arrows along the curve show the monotonously increasing direction of s. b) Geometrical information of the physical boundary which is discretized into a series of boundary pairs (a square and a circle which are located on the nearest lattice points from the boundary). Boundary conditions are reinterpreted on the zigzag (dash-dot) line

This notation means that the velocity $\mathbf{c}_i$ has its components in the $x-y$ plane given by the ith column of the matrix. We will define a particular speed as $c_s = (\Delta x/\Delta t)/\sqrt{3}$ (which would be called the sound speed in the traditional fluid problem, but here it only has a formal analogy). The direction of $\mathbf{c}_i$ is defined by the unit vector $\hat{c}_i = \mathbf{c}_i/|\mathbf{c}_i|$.

Denoting the micro distribution function as $g_i(t, \mathbf{x})$, its temporal evolution follows the two main steps:

(i) the collision step

$$g_i^*(t, \mathbf{x}) = g_i(t, \mathbf{x}) + \frac{1}{\tau}\left(g_i^{eq} - g_i(t, \mathbf{x})\right) + w_i \Delta t R \tag{5}$$

(ii) and the streaming step

$$g_i(t + \Delta t, \mathbf{x}) = g_i^*(t, \mathbf{x} - \mathbf{c}_i \Delta t) \tag{6}$$

Here g_i^* is known as the post-collision distribution function, w_i is the weight factor valued as $w_0 = 1/3$ and $w_{1,2,3,4} = 1/6$, and $\tau = 3D \cdot (\Delta t/\Delta x^2) + 1/2$ is the dimensionless relaxation time. The equilibrium distribution function is

$$g_i^{eq} = w_i c \left[1 + \frac{\mathbf{u} \cdot \mathbf{c}_i}{c_s^2}\right] \tag{7}$$

which depends on the macro concentration c and velocity $\mathbf{u}$. The relation between the micro distribution function and the macro concentration is simply given by

$$c = \sum_{i=0}^{4} g_i \tag{8}$$

It is proven via an asymptotic analysis (see Yoshida and Nagaoka (2010); Huang and Yong (2015) and Appendix Appendix A) that Eqs. (5)-(7) converge to the convection-diffusion Eq. (1) with a second-order precision when $\Delta t/\Delta x^2 \sim O(1)$. A brief derivation is provided in Appendix Appendix A. We define the dimensionless diffusivity and velocity (in the lattice Boltzmann units) as

$$\begin{aligned} D^{'} &= D \cdot \Delta t/\Delta x^2 \\ \mathbf{u}^{'} &= \mathbf{u} \cdot \Delta t/\Delta x \end{aligned} \tag{9}$$

The relaxation time τ and $D^{'}$ are related by (see Appendix Appendix A)

$$\tau = 3D^{'} + 1/2 \tag{10}$$

2.2. General Moving Boundary Condition Treatment

Since the boundary treatments on both sides of the membrane (Fig. 1) are identical from the technical point of view, we only discuss the handling of c^-. Thus below, we omit "$\pm$" sign in (3). We will split the general Robin boundary conditions given by Eq. (3) into two pieces (and then combine them in the general case). The first one is the Dirichlet condition written as

$$c = \alpha_3 \quad (\alpha_1 = 1, \alpha_2 = 0) \tag{11}$$

and the second one is the Neumann condition written as

$$\frac{\partial c}{\partial \mathbf{n}} = \alpha_3 \quad (\alpha_1 = 0, \alpha_2 = 1) \tag{12}$$

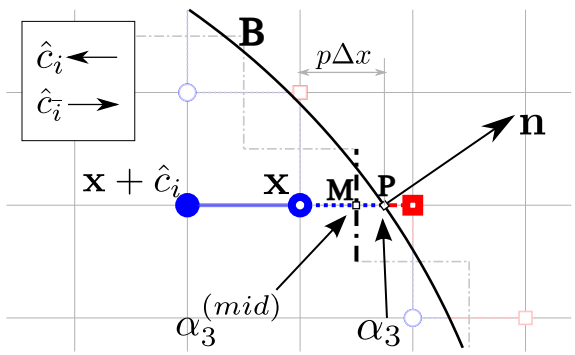

Figure 2: A typical boundary lattice is highlighted as the hollow circle. $g_i(t, \mathbf{x})$ is to be calculated from boundary condition (see text). The curved boundary needs to be interpolated onto the zigzag boundary (dashed-doted line). This process is done via finding a value $\alpha_3^{(mid)}$ imposed on zigzag boundary which is consistent with $c = \alpha_3^{(mid)}$ (Dirichlet) or $\partial c/\partial \hat{c}_{\bar{i}} = \alpha_3^{(mid)}$ (Neumann) on the curved boundary value problem. $\hat{c}_i$ is the unit vector parallel to $\mathbf{c}_i$, $\hat{c}_{\bar{i}} = -\hat{c}_i$.

2.2.1. Treatment for Static Curved Boundary

The moving boundary treatment is composed of two steps. The first one is to deal with the shape itself at a given moment (a static boundary), while the second one consists in reconstructing the boundary lattice points when they flip from one side of the membrane to the other due to the motion of the free boundary.

The static boundary treatment follows closely (with some important modifications; see below) that given in Refs. Huang and Yong (2015); Huang et al. (2016). The authors there first extended the halfway bounce-back scheme (known for fluid solvers) to the convection-diffusion LBM. This modified scheme is suitable for the type of the boundary shown by the dashed-dotted lines in Figs.

1 b and 2). For that boundary (which will be called hereafter *zig-zag* boundary) all its intersecting points with the lattice mesh segments are defined at the middle of the mesh segments (dashed-dotted lines in Figs. 1 b and 2; $\mathbf{M}$ is one representative point). Since this scheme requires only local information, it lends naturally itself to an efficient parallel implementation.

Recall that in Fig. 1 a physical boundary is discretized into a series of boundary pairs. Assuming there is a boundary lattice point that resides at position $\mathbf{x}$ (see Fig. 2, the hollow circle and hollow square provide an example of a typical boundary pair), due to the existence of boundary B, the distribution function $g_i(t + \Delta t, \mathbf{x})$ cannot be determined from streaming Eq. (6). Indeed, if $\mathbf{x}$ is the hollow blue circle, then the streaming operation given by Eq. (6) (where the argument of the right hand side is $\mathbf{x} - \mathbf{c}_i \Delta t$) would propagate the information from the hollow red square to the hollow blue circle (see Fig. 2). The streaming procedure will fail due to the presence of the boundary, and thus the determination of the evolution of g_i at a boundary point, designated by $\mathbf{x}$, requires a special treatment.

The concentration field (or its normal derivative) is specified at the real boundary (a representative point is $\mathbf{P}$ in Fig. 2) to be equal to α_3 (for Dirichlet boundary condition). The discretized boundary has a representative point denoted as $\mathbf{M}$, at which the concentration (still unknown) is denoted as $\alpha_3^{(mid)}$. Below we show how is this value determined from α_3 and the concentration field at point $\mathbf{x}$. Once this task is performed, we have at our disposal the concentration field inside the domain of interest, satisfying the boundary condition. The

idea is then to use the Boltzmann equation in order to determine the sought-after micro-distribution appearing on the left hand side of Eq.(6) as a function of the post-collision distribution at point $(t, \mathbf{x})$ and the macro concentration field at the discretized boundary (Eq. (13)). The proof is given in the Appendix Appendix B and the result is given by (for Dirchlet and Neumann conditions)

$$\begin{cases} g_i(t+\Delta t, \mathbf{x}) = & -g_{\bar{i}}^*(t, \mathbf{x}) + & \frac{1}{3}\alpha_3^{(mid)} & \text{for} & c = & \alpha_3^{(mid)} \\ g_i(t+\Delta t, \mathbf{x}) = & \frac{1+3\mathbf{u}\cdot\hat{c}_i}{1-3\mathbf{u}\cdot\hat{c}_i} g_{\bar{i}}^*(t, \mathbf{x}) + & \frac{D^{'}\Delta x}{(1-3\mathbf{u}\cdot\hat{c}_i)}\alpha_3^{(mid)} & \text{for} & \hat{c}_i\cdot\nabla c = & \alpha_3^{(mid)} \end{cases} \tag{13}$$

The streaming equation given by Eq.(6) is substituted by the above equation for any lattice point $\mathbf{x}$ lying next to the boundary. Our analysis presented in Appendix Appendix B shows that the scheme has a second-order precision. This is consistent with the direct numerical estimates Huang and Yong (2015).

Let us now show how to determine $\alpha_3^{(mid)}$. An interpolation procedure was developed in Huang et al. (2016) for such a purpose, but it requires information from several lattice points. In addition, the selection of interpolating points is geometry-dependent. A simpler procedure is required for a practical implementation of moving boundaries and parallel computation. Here, we only use a single neighboring lattice point ($\mathbf{x} + \mathbf{c}_i\Delta t$ in Fig. 2).

Interpolate $\alpha_3^{(mid)}$ for Dirichlet condition.

We perform a simple linear interpolation. Let us define the normalized distance p (Fig. 2) between points $\mathbf{x}$ and $\mathbf{P}$. The idea is to use the concentration gradient at $\mathbf{x}$ at previous time step to linearly interpolate $\alpha_3^{(mid)}$ out of the

concentration field (or its derivative) at the real boundary (where $c = \alpha_3$ for a Dirichlet condition) and at $\mathbf{x}$. The concentration at point $\mathbf{M}$ and at time $t + \Delta t$ is given by

$$\alpha_3^{(mid)} = \begin{cases} \alpha_3 + (p - \frac{1}{2})\Delta x \hat{c}_i \cdot \nabla c(t, \mathbf{x}) & \text{if} \quad p \leq \frac{1}{2} \\ \frac{\alpha_3}{2p} + (1 - \frac{1}{2p}) c(t, \mathbf{x}) & \text{if} \quad p > \frac{1}{2} \end{cases} \tag{14}$$

This interpolation has a second-order precision. The separation into two cases ($p > 0.5$ and $p < 0.5$) is dictated by numerical stability.

Asymptotic analysis shows that the concentration gradient can be reconstructed locally in terms of the micro-distribution with one-order precision procedure Yoshida and Nagaoka (2010); Huang et al. (2016)

$$\nabla c = \frac{1}{\Delta t c_s^2} \left[\mathbf{u} c - \sum_{i=0}^{4} \mathbf{c}_i g_i \right] + O(\Delta x) \tag{15}$$

Interpolate $\alpha_3^{(mid)}$ for Neumann condition.

Since the zigzag boundary has its normal vector $\hat{c}_{\bar{i}}$ which is different from $\mathbf{n}$, the reconstruction of $\alpha_3^{(mid)}$ involves tangential derivative as well. It is easily seen that

$$\begin{aligned} \alpha_3^{(mid)} &= \frac{\partial c}{\partial \hat{c}_{\bar{i}}} \\ &= \hat{c}_{\bar{i}} \cdot \mathbf{n} \left. \frac{\partial c}{\partial \mathbf{n}} \right|_{\mathbf{M}} + \hat{c}_{\bar{i}} \cdot \mathbf{t} \left. \frac{\partial c}{\partial \mathbf{t}} \right|_{\mathbf{M}} \end{aligned} \tag{16}$$

The normal derivative at $\mathbf{M}$ can be obtained from $\mathbf{P}$ and first order extrap-

olation from $\mathbf{x}$,

$$\left.\frac{\partial c}{\partial \mathbf{n}}\right|_{\mathbf{M}} = \begin{cases} \alpha_3 + (p - \frac{1}{2}) \left(\left.\frac{\partial c}{\partial \mathbf{n}}\right|_{\mathbf{x}} - \left.\frac{\partial c}{\partial \mathbf{n}}\right|_{\mathbf{x}+\hat{c}_i} \right) & \text{if } p \leq \frac{1}{2} \\ \frac{\alpha_3}{2p} + (1 - \frac{1}{2p}) \cdot \left.\frac{\partial c}{\partial \mathbf{n}}\right|_{\mathbf{x}} & \text{if } p > \frac{1}{2} \end{cases} \tag{17}$$

The tangential derivative of c at point $\mathbf{M}$ is unknown, so we will express it in terms of the value at $\mathbf{x}$ and at the neighboring point $\mathbf{x} + \hat{c}_i$. A linear extrapolation yields

$$\left.\frac{\partial c}{\partial \mathbf{t}}\right|_{\mathbf{M}} = \left.\frac{\partial c}{\partial \mathbf{t}}\right|_{\mathbf{x}} + \frac{1}{2} \left(\left.\frac{\partial c}{\partial \mathbf{t}}\right|_{\mathbf{x}} - \left.\frac{\partial c}{\partial \mathbf{t}}\right|_{\mathbf{x}+\hat{c}_i} \right) \tag{18}$$

Finally, we consider the general Robin boundary condition, which is a linear combination of Dirichlet (Eq. (11)) and Neumann (Eq. (12)) boundary conditions. It reads

$$\alpha_1 c + \alpha_2 \frac{\partial c}{\partial \mathbf{n}} = \alpha_3 \tag{19}$$

Similar to Huang et al. (2016), we reduce the Robin condition back to a Neumann problem by approximating the boundary concentration c in the term $\alpha_1 c$ in Eq. (19) with its value at previous time step. Since the boundary position is off-lattice (see point $\mathbf{P}$ in Fig. 2), the value of c on the boundary is evaluated with concentration value on the nearest boundary lattice and corresponding gradient information (see Eq. (15)). Recalling the diffusive scaling assumption mentioned at the end of section 2.1, namely $D^{'} = \frac{\Delta t}{\Delta x^2} D \sim O(1)$, it is obvious that the introduced error by this approximation merely introduces a second order error term.

2.3. Treatment of the Moving Boundary

When dealing with an interface two questions arise: (i) how is the inter-

face being advanced in the course of time, and (ii) how is the interface being discretized and the boundary conditions implemented. The first point is quite classical: once the velocity field is known then the interface is simply advected by the local velocity (using Euler scheme). In this case the velocity is defined on the fluid lattice, whereas the interface is off-lattice. In order to transfer the fluid velocity information from the lattice to the interface the immersed boundary method is used Peskin (2002); Feng and Michaelides (2004); Yang et al. (2009); Shen et al. (2017). This is what we adopt here for the fluid flow only (but not for the solute). For the diffusion problem, we have to specify how is the boundary condition imposed on the interface. The first step is to determine the discretized interface as described in Fig. 1. This procedure is different from the IBM, since our interface is defined as a geometrical one (a sharp interface description) and not as a thin strip as is the case with the IBM . The reason for this treatment is that, unlike the velocity field, the concentration field (and its derivatives) is generically discontinuous at the interface, so that the IBM is inappropriate for handling this situation with enough precision. Some exceptions are observed for a special type of boundary conditions as described in Huang et al. (2009); Lee et al. (2010,?); Chen and Lai (2014). Once the interface is discretized the boundary terms are evaluated and then transfered to the concentration lattice points in order to deal with the LBM at the interfacial region (see Eq. 13).

After each interface motion (obtained thanks to the fluid velocity) we have to

resolve the problem of points flipping from one side of the interface to the other side. A possible type of treatment is the so-called refilling procedure Lallemand and Luo (2003). In this method, a point which passes from one side to the other has to be connected to new neighbors located on the same new side. The new distribution function value of the point having passed the interface is evaluated as an extrapolation from its new neighbors. Here we will use a similar strategy but in a more refined manner, as described below. Our procedure is split into three steps: (a) at a given time we have configuration shown in Fig. 3a with 4 boundary lattices (shown with empty red squares). At this moment the boundary treatment is done as if the boundary were fixed at that configuration. (b) At later time the boundary moves to configuration shown in Fig. 3b where, for example, a new boundary point (in addition to the previous four), shown with empty magenta square, enters the domain. In Lallemand and Luo (2003) the distribution function of the new boundary point is obtained by extrapolation from its neighbors shown in red in Fig. 3b. Our treatment is slightly different. The idea is to ignore first that new point (since we do not yet dispose of the value of its distribution function), and take into account the boundary motion thanks to the new 4 distances that the 4 red square points make with the new boundary position. We then calculate the distances p for each of the boundary neighboring points (p was described previously in Fig. 2, and was represented in Fig. 3 with a red dashed line) and evaluate the boundary conditions according to Eqs. (13 to 17). (c) In the third step, we evaluate the distribution function at the new point (shown with a hollow magenta square in Fig. 3c) by using

information from its neighbors, as explained below.

The natural neighbor interpolation based on Voronoi tessellation Novak and Slepchenko (2014) or linear/quadratic interpolation Lallemand and Luo (2003) could be implemented. In order not to introduce too many branching operations into moving boundary treatment, we used a simple linear interpolation instead (which lends itself to efficient parallel implementation and is robust even when the membrane undergo high distortions). Our analysis has led us to postulate the following relation for the distribution function at the new points swept by the boundary

$$g_k = \frac{\sum_{k' \in S^{(ref)}} w_{k'} (2g_k(t, \mathbf{x} + \mathbf{c}_{k'}) - g_k(t, \mathbf{x} + 2\mathbf{c}_{k'}))}{\sum_{k' \in S^{(ref)}} w_{k'}} \tag{20}$$

Here $S^{(ref)}$ is a collection of subscripts defined on a lattice point , which flipped from Ω^+ to Ω^- in the new time step (see Fig. 3). An index k belongs to $S^{(ref)}$ only if both $\mathbf{x} + \hat{c}_k$ and $\mathbf{x} + 2\hat{c}_k$ belongs to $\Omega^-(t)$ and $\Omega^-(t + \Delta t)$ in both previous and present time step. We have postulated equation (20) from linear extrapolations and a set of intuitive weight factors as defined in section 2.1. We have successfully tested these weight factors by a number of numerical experiments (examples of validation will follow). Similar extrapolations (for rigid moving boundaries) were adopted for fluid and solute problems in Yin et al. (2012); Chen et al. (2013a).

Finally, note that in all cases treated here the boundary conditions for the solute are periodic along the x-direction, and are various in the y-direction, such as periodic, or absorbing walls (see examples below),

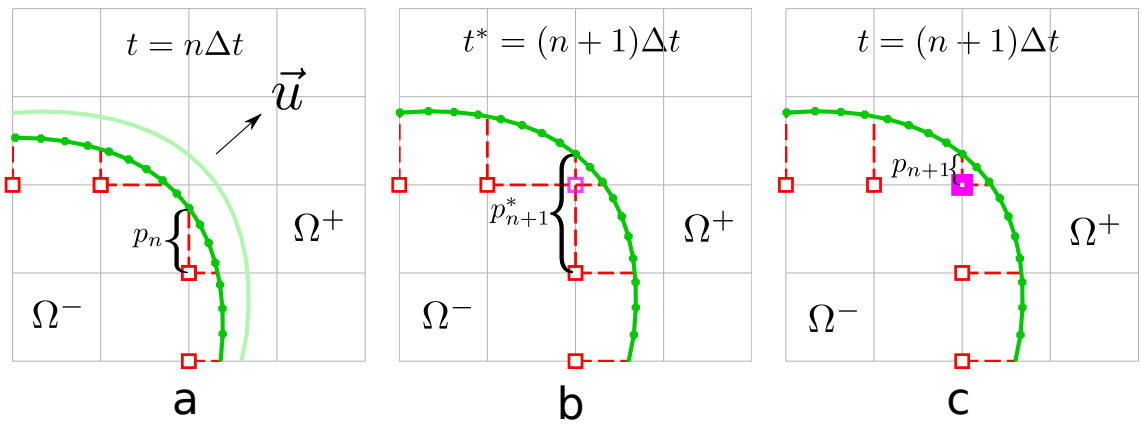

Figure 3: The procedures dealing with the moving boundary problem: (a) at that time step, we treat the boundary condition as a static boundary. (b) at intermediate time step, keep the boundary grids fixed, calculate the intersection length p due to boundary movement (defined in Fig. 2), and deal with the new boundary condition with the p value (even if it is larger than 1). (c) Search for neighboring lattice points in the set $S^{(ref)}$, and then calculate the new distribution function value via Eq. (20)

depending on applications. The method developed here lends itself to other boundary conditions. For example, other boundary conditions for the solute at the external boundaries could be used as well, such as the Robin ones, and so on.

3. Validations

3.1. Validations on time-dependent problems with static boundaries

3.1.1. A pure diffusion problem in an irregular domain

We first validate our boundary condition scheme by treating a time-dependent diffusion problem in the presence of a static boundary. This problem has an analytical solution Hu et al. (2018). A periodic square domain is defined as $\Omega = [-1, 1] \times [-1, 1]$, with the presence of an internal boundary

$$\mathbf{B} = [r(\theta)\cos(\theta), r(\theta)\sin(\theta)],\ \theta \in [0, 2\pi)$$

here $r(\theta) = 0.4 + 0.1\cos(3\theta)$. As the internal boundary is closed, it divides Ω into Ω^- and Ω^+, which are the external and internal domains respectively. We focus here on the solution in Ω^-. The analytical solution is given by Hu et al. (2018)

$$c^{(ana)}(t, x, y) = 1 + 0.5\exp\left(-2\pi^2 t D_a\right)\cos(\pi x)\cos(\pi y) \text{ for } (x, y) \in \Omega^-$$

Here D_a is a dimensionless diffusion coefficient. For definitness, its value is set here to 0.1. The above solution is valid for both Dirichlet and Neumann

conditions The above concentration field satisfies the pure diffusion equation with initial condition

$$c|_{t=0} = c^{(ana)}(0, x, y)$$

and a corresponding Dirichlet type boundary condition

$$c|_{\mathbf{B}} = c^{(ana)}$$

or a Neumann type boundary condition

$$\left.\frac{\partial c}{\partial \mathbf{n}}\right|_{\mathbf{B}} = \partial_{\mathbf{n}} c^{(ana)}$$

Here $\mathbf{n}$ is the normal vector pointing from Ω^- to Ω^+. We tested numerically both boundary conditions.

The choice of relaxation time τ in simulation is quite flexible. As we have seen in Eq. (9) and Eq. (10), once the lattice mesh size Δx and relaxation time τ are fixed, the total number of the simulation steps is given by

$$N^{(step)} = \frac{T}{\Delta t} = \frac{T D_a}{\Delta x^2 D'} = \frac{3 D_a}{\Delta x(\tau - 0.5)} \cdot T$$

For definiteness, we fixed $T = 1$ (in an arbitrary unit). Simulations with different values of relaxation time were tested, namely $\tau = 0.625, 0.75$ and 1. The numerical results are then compared to the analytical solution $c^{(ana)}$ at this particular time $T = 1$. We define the numerical relative error of concentration $c^{(num)}$ as

$$E(\Delta x) = \frac{||c^{(num)} - c^{(ana)}||}{||c^{(ana)}||} \tag{21}$$

where $||\cdot||$ is the euclidean norm (the L^2-norm defined as $||f|| \equiv [\int_\Omega f(x,y)^2 dxdy]^{1/2}$). A second-order convergence is observed (see Fig. 4).

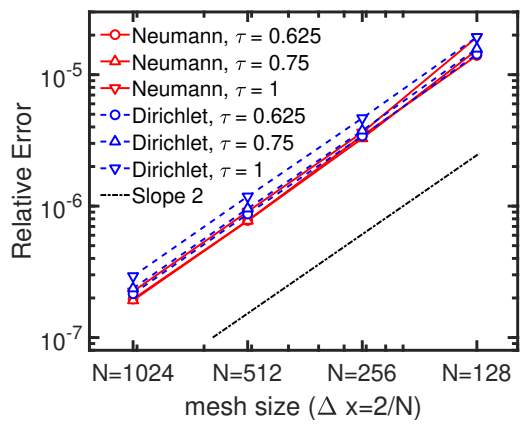

Figure 4: The relative error against the mesh size in the static three-leaves problem from Hu et al. (2018).

3.1.2. An advection diffusion problem in an irregular domain

Secondly, we test this boundary condition scheme against an advection diffusion problem in an irregular domain, which has an analytical solution Huang et al. (2016). The computational domain is defined as $\Omega = \{(x, y) \in \mathbb{R}^2 | \phi(x, y) < 0\}$, here $\phi(x, y)$ is a scalar field which reads

$$\phi(x, y) = x^4 - 5x^2 - 3x + 2y^4 - 6y^3 - y - 1$$

The time dependent advection diffusion problem is governed by

$$\frac{\partial}{\partial t} c(t, x, y) + \nabla \cdot (\mathbf{u}c) = \nabla \cdot (D \nabla c) + S, \ (x, y) \in \Omega, , \ t \in [0, T]$$

The velocity field is set to be a constant, $\mathbf{u} = (1, 0)$ and D is a constant scalar. The time dependent source term S is

$$S = (x^3 + y^3)\omega \cos(\omega t) + [3x^2 - D(6x + 2)] \sin(\omega t)$$

The initial condition is given as

$$c|_{t=0} = 0,\ (x, y) \in \Omega$$

The boundary condition, which is defined on the zeros of $\phi(x, y)$, can be defined as either Neumann type or Robin type. For Neumann condition, it reads as

$$\left.\frac{\partial c}{\partial \mathbf{n}}\right|_{\phi=0} = (3n_x x^2 + 2n_y y)\sin(\omega t)$$

For Robin condition, it is given by

$$\left.\left(c + \frac{\partial c}{\partial \mathbf{n}}\right)\right|_{\phi=0} = (x^3 + y^2 + 3n_x x^2 + 2n_y y)\sin(\omega t)$$

Here n_x and n_y are components of the normal vector pointing outward. This problem has an analytical solution

$$c = (x^3 + y^2)\sin(\omega t)$$

By following Huang et al. (2016), we set $D = 1$ and $\omega = 1$. A computational domain $[-3, 3] \times [-2, 4]$ is uniformly meshed into $N \times N$ lattices. For the Robin condition, the value of c on the boundary is obtained by the values at the boundary lattices and the gradient information (see Eq. (15)) at previous time step. By choosing different τ and mesh size $\Delta x = 6/N$, the numerical results at $T = 1$ are compared with the analytical solution. A second order convergence is observed (see Fig. 5). Despite the fact that there is only a single neighboring point to a given boundary lattice point and no curvature information (recall Fig. 2) used in this boundary treatment, the relative error is of the same magnitude compared to the results from Huang et al. (2016) (recall that in that work

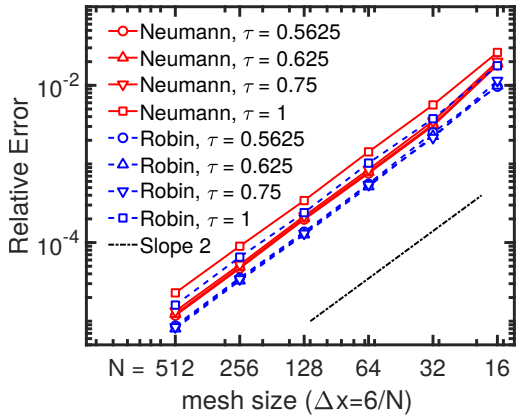

Figure 5: The relative error against the mesh size in the advection diffusion problem in an irregular domain from Huang et al. (2016).

several neighboring points and boundary curvature information are employed). **The relative error against the different choices of relaxation time τ (and thus against diffusivity, see eq. 10) is gathered in Fig. 6. This result suggests that a choice for the relaxation time in the range $\tau \leq 1$ (see Fig. 6) is an appropriate one. Our numerical experiments revealed that this choice favors stability. Indeed, we found that for both Neumann and Robin type boundary condition, simulations with a large relaxation time led to numerical instability (e.g. the choice $\tau = 3$ and $N = 16$ led to divergence). We identified that the instability results from extrapolation of tangential gradient in Eq. (18). Note that omitting the extrapolated term can make the simulation more stable with large relaxation time but as a counterpart the precision of the boundary treatment will degrade down to first-order.**

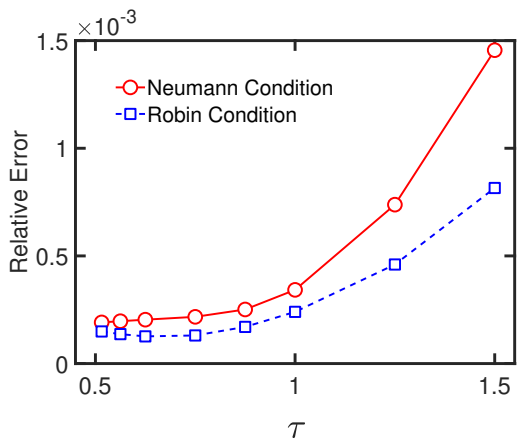

Figure 6: The relative error against relaxation time τ in the advection diffusion problem in an irregular domain from Huang et al. (2016). The lattice mesh size is fixed as $N = 128$.

3.2. Moving Boundary Validation

Now we perform some validation tests on a problem with moving boundaries. The first example is a cylinder (which is a circle in 2D, which encloses a solute) which is advected by a constant velocity. The second case consists of a deformable opaque surface that encloses a solute and which is distorted by a rotational velocity field.

3.2.1. An Advected Leaking Rigid Reservoir

Consider a cylindrical reservoir which is advected by a constant velocity $\mathbf{u}_0$ in a periodic box $\Omega = [-a/2, a/2] \times [-b/2, b/2]$. The boundary of the advected reservoir is described as

$$\mathbf{B}(t, \theta) = [r_0 \cos(\theta) + u_{0x} t, -r_0 \sin(\theta) + u_{0y} t] \, , \, \theta \in [0, 2\pi)$$

where r_0 is the radius of the cylinder. A solute concentration field c is defined in Ω and obeys

$$\frac{\partial}{\partial t}c(t,x,y) + \nabla \cdot (\mathbf{u}_0 c) = \nabla \cdot (D\nabla c),\ (x,y) \in \Omega, t \in [0,T]$$

The initial condition is set as

$$c_{ini} = \begin{cases} 1 & \text{inside reservoir} \\ 0 & \text{outside reservoir} \end{cases}$$

The concentration along the internal and external sides of $\mathbf{B}$ are denoted as $c^-(t,\theta)$ and $c^+(t,\theta)$ respectively. The normal vector points into the outward direction. The solute is leaking from the reservoir into the external zone, and this leakage is described by the following boundary condition at the cylinder surface

$$D\frac{\partial c^-}{\partial \mathbf{n}} = -D\frac{\partial c^+}{\partial \mathbf{n}} = k(c^- - c^+)$$

Parameters are fixed as $r_0 = 0.8$, $a = 4$, $b = 2$, $D = 1$, and $k = 1$. The concentration fields computed with two different constant velocities $\mathbf{u}_0 = [a/T, 0]$ or $[0,0]$ are compared at $T = 1$. The contour plots of the numerical solution with $\Delta x = b/512$ is shown in Fig.7

The boundary concentration values, c^- and c^+, are evaluated thanks to the concentration values and their gradients at the lattice points (see Eq. (15)). Since $\mathbf{u}_0$ is constant, one can infer from Galilean invariance that the actual concentration field in the case where $\mathbf{u} = [a/T, 0]$ should be identical to that obtained in the case with zero advection velocity. However, the numerical errors may affect the Galilean invariance. Therefore, it is important to check if this

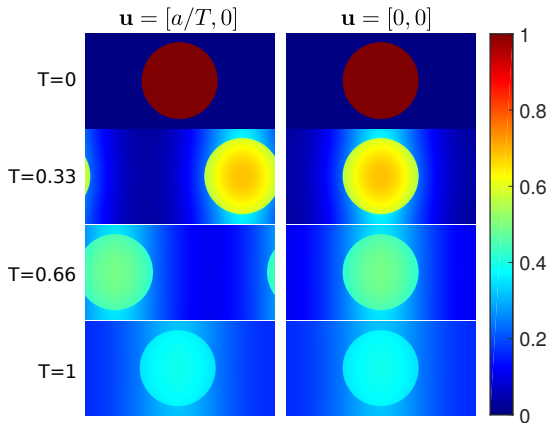

Figure 7: Snapshots for the concentration field for $\mathbf{u} = [a/T, 0]$ (left side) and $\mathbf{u} = [0, 0]$ (right side) respectively. In both simulations, we have set $\Delta x = b/512$ and $\tau = 1$. Since the only difference between the left side simulation and the right side one is that the concentration field is advected by a constant velocity, it should be identical to the concentration field on the right side up to a translation (Galilean invariance). This property is accurately reproduced in this simulation, although the LBM is based on an Euclidian mesh. The preservation of Galilean invariance is crucial to scenarios with long term advection such as cell membrane flowing in channels of realistic length.

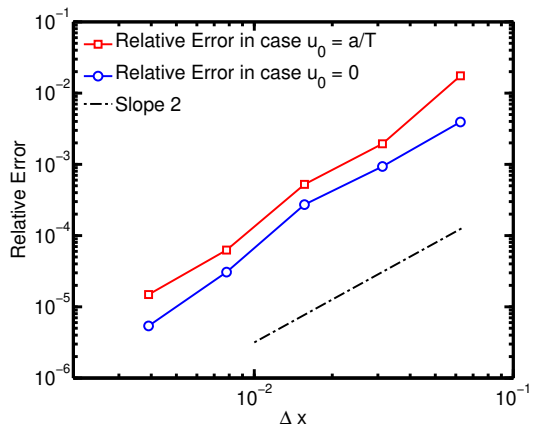

Figure 8: Relative error against Δx in the case of a cylindrical reservoir being advected by a constant velocity

property is preserved after long simulation time (see the comparison of the two results at $T = 1$ in Fig. 7). τ is fixed to 1 in these simulations. The numerical solution for $\Delta x = b/1024$ and $\mathbf{u}_0 \equiv \mathbf{0}$ is used as a reference solution from which the error is calculated when non zero velocities are considered. A second-order convergence is obtained (Fig. 8).

3.2.2. A Reservoir that undergoes rotation and distortion

In this case we consider a divergence-free rotational velocity field $\mathbf{u} = [u_x, u_y]$ (see the vector field in Fig. 9 colored in gray) in a simulation box $\Omega = [-1, 1] \times [-1, 1]$.

$$\begin{cases} u_x = & -0.5[1 + \cos(\pi x)]\sin(\pi y) \\ u_y = & 0.5[1 + \cos(\pi y)]\sin(\pi x) \end{cases}$$

A localized circular reservoir is initially defined with its centroid at $\mathbf{x}_0 =$

$[0.5, 0]$ with radius $r_0 = 0.3$. Its boundary is denoted as $\mathbf{B}$. The reservoir is then subjected to a rotating velocity field, thus, the motion of the reservoir boundary is expressed as $\partial \mathbf{B}/\partial t = \mathbf{u}$. A concentration field c is defined on this simulation box, and is governed by the advection-diffusion equation A zero-flux Neumann condition is imposed on both sides of the reservoir boundary $\mathbf{B}$. A representative Dirac delta function is used as an initial condition $c_0 = \delta(\mathbf{x} - \mathbf{x}_0)$. **More precisely, we consider a regularized Dirac function in the form of Gaussian function with a width of order of two lattice points**. We set the Peclet number to $Pe = \max(|\mathbf{u}|)/D = 50$. The imposed velocity field is expected to extremely elongate and distort the reservoir. This extreme distortion will constitute an interesting test of the code robustness. The advancing of the distorted reservoir boundary is conducted by means of a $4th$ order Runge Kutta method, under which, the numerical error of reservoir area is adequately suppressed. A numerical solution (obtained with via $\Delta x = 1/512$ and $\tau = 0.75$) is presented in Fig. 9. We measure the error at $T = 1$, when the shape is still easily resolvable for a large enough mesh size $\Delta x = 1/16$. The finest mesh $\Delta x = 1/2048$ is used to estimate the relative error. (21). A convergence rate between first and second order (around 1.45, see Fig. 10) is observed. We attribute this to the loss of resolving geometry information when the mesh size is not small enough. For example, in the case where $\Delta x = 1/32$, in Fig. 10, the maximum width of the shape is represented by only 7 lattice points, which may cause a significant inaccuracy during the reconstruction process of the zigzag numerical boundary. Despite the relative degradation of the quality

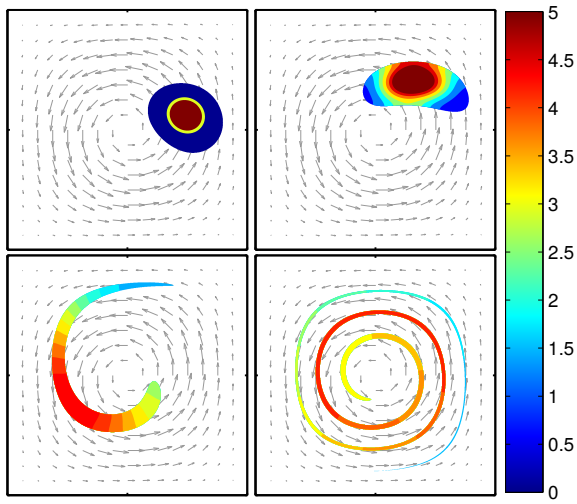

Figure 9: From left to right, up to bottom we show the numerical solution of the concentration field at $T = 0.125$, 0.5, 2 and 8, in which $\Delta x = 1/512$. The vector fields in gray represent the rotational velocity field.

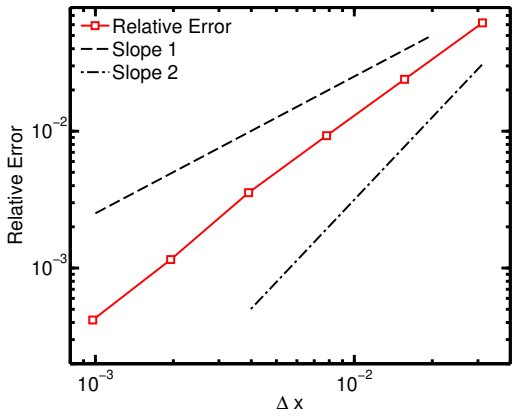

Figure 10: Relative error against Δx in the case of a cylindrical reservoir being advected and distorted by a rotational velocity field $\mathbf{u}$

of precision (from the expected order 2 down to order 1.5) the code robustly handles extreme distortions, such as the situation shown at $T = 8$ in Fig. 9.

4. The Arteriole Thrombosis Drug Delivery Simulation

The validations (section 3) have proven that the numerical method's capability of dealing with advection, rotation and distortion of a moving boundary, with even quite ample deformation patterns under flow. We now implement this solver for the study of a first practical example, the arteriole thrombosis drug delivery. This example is inspired by previous numerical studies on simplified models for liposome drug release in channel flow Gekle (2017); Kaoui (2018). We consider a liposome that encapsulate some drug to be released in a blood vessel. We take here into account both the plasma fluid and the RBCs. We follow below closely the work of Kaoui Kaoui (2018).

Liposomes are closed membranes, and are considered as promising targeted drug carriers. They have typical diameters ranging from 100 nm to $1\mu m$ Sercombe et al. (2015). They are suitable means for carrying hydrophilic drugs to a particular location in the organism where they may release their content thanks to an external stimulus (for example ultrasound excitation) or when the surrounding fluid shear stress reaches a critical value (shear stress is the highest in arterioles). Although there exist various types of liposomes depending on the precise purpose, we consider it here to be composed of a single lipid bilayer. Actually in 2D and for an incompressible membrane there is only a single mode of deformation (bending), and there is no real distinction between different models

(vesicle, capsule, red blood cell, etc...).

We consider a straight long channel for the arteriole model, with a Gaussian hill shaped obstacle on one side of the vessel wall to represent the thrombosis (Fig. 11). We adopt a 2D vesicle as a crude model for RBCs (we will nevertheless use the abbreviation RBC in what follows). An immersed boundary coupled lattice Boltzmann method is employed to resolve the fluid-membrane coupled system. This means, that the motion of the RBCs is performed by the classical immersed boundary method (unlike the treatment of the diffusion problem) Peskin (2002); Feng and Michaelides (2004); Yang et al. (2009); see Shen et al. (2017) for details of our fluid solver. A liposome is initially located at the upstream of a thrombosis site, surrounded by RBCs. The liposome encapsulates a water-soluble drug with concentration $c_0 = 1$. Its membrane is initially impermeable to the drug. Then the liposome is advected by blood flow until it reaches a particular distance from the thrombosis, where we assume that the liposome membrane becomes suddenly absolutely permeable to solute (mimicking the effect of an external stimulus). A schematic representation is given in Fig. 11 to show the simulation layout.

We would like to evaluate how does the presence of RBCs impact the drug delivery process. The role of RBCs is two-fold, they affect the flow field, and they serve as solute obstacles. To elucidate the role of each effect we consider 3 different situations, one without RBCs at all, the second one with passive RBCc (i.e. RBCs are completely transparent to the drug), and finally a realistic case in which the RBCs are opaque to the drug. In all the three cases we consider a

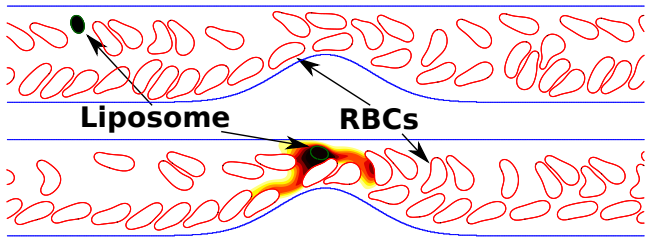

Figure 11: A schematic representation of liposome drug delivery process near an arteriole thrombosis. The top panel represents some time before drug release, and the bottom one represents the situation after drug release. The colormap represents the concentration of drug solute. The liposome becomes transparent after it reaches a particular distance from the thrombosis

complete absorption condition along the vessel walls (zero-value Dirichlet condition). When RBCs are considered as opaque to solute, the boundary conditions at the RBC membrane and at the wall reads

$$\begin{cases} \dfrac{\partial c}{\partial \mathbf{n}} = 0 & \text{on RBCs membrane} \\ c = 0 & \text{on vessel walls} \end{cases} \tag{22}$$

When we consider a transparent RBC model, we relax the first of the two above boundary conditions. In that case the RBCs only affect the flow pattern, which in turn affects the advection of the solute, but the RBCs do not affect directly the solute (no solute obstacle).

4.1. Preliminaries on the fluid–membrane–solute system

We first briefly recall the modeling of 2D membrane problem, which serves to model RBCs and the drug carrier as well. A 2D unstretchable closed membrane is used for the RBC model, and has a bending elastic modulus $\kappa_b = 3 \times 10^{-19} J$

Betz et al. (2009); Kaoui et al. (2011). The membrane force is obtained from the Helfrich energy

$$H(\mathbf{X}(t,s)) = \frac{\kappa_b}{2}\oint \kappa^2 ds + \oint \zeta ds$$

Here $\mathbf{X}(t,s)$ is the position of RBC membrane, κ is the local curvature, ζ is a Lagrange multiplier that enforces local membrane inextensibility, and s is the curvilinear coordinate. The membrane force (which is obtained as a functional derivative of H with respect to $\mathbf{X}(t,s)$) is applied as a bulk force (albeit localized close to the membrane, in an immersed boundary spirit) to the fluid

$$\rho\left(\frac{\partial \mathbf{u}}{\partial t} + \mathbf{u}\cdot\nabla\mathbf{u}\right) = -\nabla p + \nabla\cdot\left[\eta(\nabla\mathbf{u} + \nabla\mathbf{u}^T)\right] + \oint \frac{\delta H}{\delta \mathbf{X}}\cdot\delta(\mathbf{x}-\mathbf{X})ds,$$

where the supescript T stands for the transposition operation. **The membrane force (which is the functional derivative with respect to the membrane position) is given by Kaoui et al. (2008)**

$$\mathbf{f}_{\text{mem}\to\text{flu}} = \kappa\left(\frac{d^2\kappa}{ds^2} + \frac{1}{2}\kappa^3\right)\mathbf{n} - \zeta\kappa\mathbf{n} + \frac{d\zeta}{ds}\mathbf{t} \tag{23}$$

Then, the velocity field $\mathbf{u}$ is used to advance the membrane shape

$$\frac{\partial \mathbf{X}}{\partial t} = \int \delta(\mathbf{x}-\mathbf{X})\mathbf{u}(\mathbf{x})dxdy$$

We define the Capillary number as $Ca = \mu_{ex}\dot{\gamma}_w R_0^3/\kappa_b$, where η is the fluid viscosity (which is position dependent, so that it can be taken to be different inside and outside of the RBC, if need be; see later). $\dot{\gamma}_w$ is the flow shear rate at channel wall in the absence of thrombosis, liposome and RBC, R_0 is a characteristic radius of the RBC, $R_0 = \sqrt{A/\pi}$. A reduced RBC area is defined

as $RA = 4\pi A/P^2$, A and P are constant area and perimeter, respectively. RA is an index that quantifies the roundness of the RBC, and taken here as $RA = 0.7$. For the RBC model we take $R_0 = 3\mu m$, whereas for the drug carrier (liposome, for which we adopt the same membrane model as the RBC) we take $RA^{(lip)} \approx 0.997$ (a quasi-circular shape) and a radius $R_0^{(lip)} = 1.8\mu m$. We set $Ca = 10$, meaning that the flow strength is large enough to strongly deform RBCs. This will allow us to test the robustness of the code. In the whole simulation we keep the Reynolds number $Re = max(|\mathbf{u}|)R_0^{(ves)}/\eta \approx 0.2$. The channel width and length are $W = 7.5R_0^{(ves)}$ and $L = 75R_0$, thus the simulation box is $\Omega^{(vessel)} = [-37.5R_0, 37.5R_0] \times [-3.75R_0, 3.75R_0]$. The Hematocrit value 31.3% is taken for RBCs, which corresponds to 56 representing cells in the channel. The thrombosis is shaped as

$$y = h_t \cdot exp\left[-\frac{1}{2}\left(\frac{x - L/2}{w_t}\right)^2\right]$$

Here $h_t = 0.5 \cdot W$ and $w_t = W$ are the height and the width of the shape.

Several studies Zhao et al. (2012); Kumar and Graham (2012); Gekle (2016); Müller et al. (2016); Krüger (2016); Guckenberger and Gekle (2018) have shown that due to the small liposomes size, their rigidity and flow conditions, the margination (caused by RBCs) effect will drive them to the so called cell-free layer (CFL) near the vessel wall. Our long term simulation also confirmed this tendency. However, in the absence of RBCs, the liposome remains at its initial lateral position while being advected by the flow along the channel. In order to be able to compare the results with those obtained in the presence of RBCs (where margination prevails) we selected the initial liposome position to be in

the CFL (as in the presence of RBCs), $1.25R_0$ distant from the upper vessel wall. We use the following criterion for drug release: the liposome is impermeable to solute until its centroid reaches a given distance from the thrombosis, below which it becomes transparent. In these simulations we have set that distance to be $x^{(permeation)} = -17.5R_0$. We have in mind the situation where the liposome develops small pores that allows solute release, whereas the liposome maintain its overall membrane integrity.

We set $\Delta x = 0.15\ \mu m$ and $Pe = max(|\mathbf{u}|)R_0^{(ves)}/D = 10$ and 100, which corresponds to typical drug solute diffusivities D (10^{-10} and $10^{-11}\ m^2/s$). Prior to the study of interest (0 value Dirichlet condition in Eq.(22), we have tested our code with zero-flux boundary condition on vessel walls in order to check numerically the mass conservation. We have found that loss of mass is always smaller than 1.5%.

4.2. Results

The solute absorption rate by vessel walls is shown for different cases in Fig. 12 (a). The normalized absorption rate is defined as

$$R(t) = 1 - \frac{\iint c(t)dxdy}{\iint c(0)dxdy} \tag{24}$$

The integration is treated as a summation among all pixels, which introduce an error term of order 1% only.

It is found that for both $Pe = 10$ and 100, whether we have transparent RBCs or no RBcs at all (solid lines and dashed lines in Fig.12 (a)) the absorption rate is practically the same. We believe this is due to the liposome's lateral

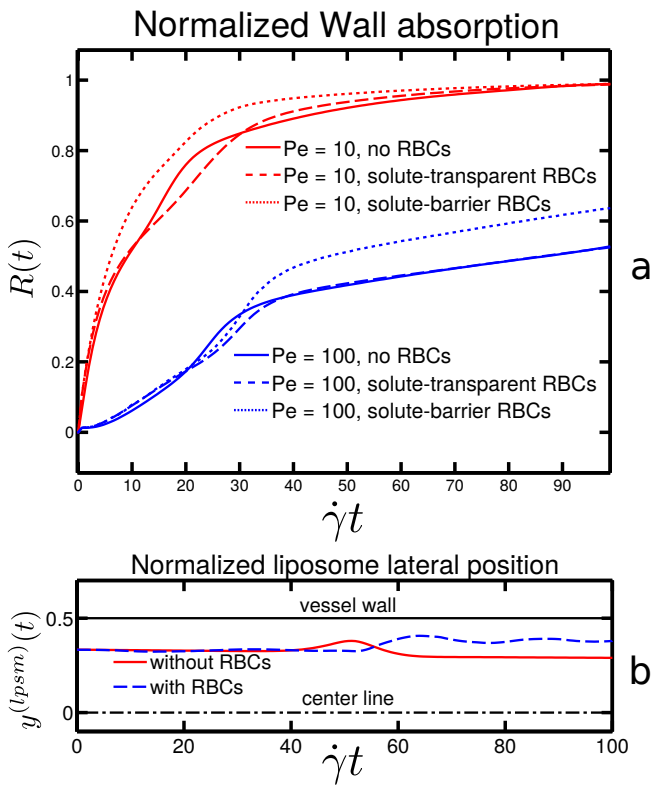

Figure 12: (a) The solute absorption rate as a function of time for $Pe = 10$ and 100. (b) The normalized lateral position of the liposome as a function of time with or without RBCs' presence. In both cases the liposome is close to the wall. The vessel wall is at position 0.5 and the center-line at position 0.

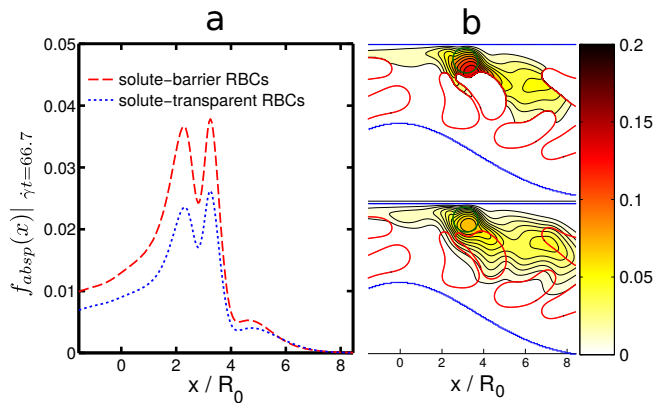

Figure 13: (a) The normalized absorption rate along the upper wall, calculated from Eq. (25). (b) Corresponding solute concentration distribution at $\dot{\gamma}t = 66.7$, both in the presence and absence of RBC; $Pe = 100$.

position near the vessel wall (Fig. 12 (b)), where the normalized distance between liposome centroid and the wall $y^{(lpsm)}(t)$ is always small enough, so that the absorption curve is diffusion-dominated, rather than advection-dominated. However, when RBCs are opaque, we find an increased absorption, shown by dotted lines in Fig. 12 (a)). A close inspection suggests that RBCs, as solute barrier, obstruct the diffusion of solute from liposome to the channel center. Consequently the gradient is increased towards vessel wall; it is proportional to the normalized absorption rate along the upper wall:

$$f_{absp}(t,x) = -\frac{D}{\dot{\gamma}R_0}\frac{\partial c}{\partial y}\bigg|_{y=3.75R_0} \tag{25}$$

Figure 13 shows the absorption rate together with RBCs configuration and the solute pattern at the thrombus location. Here again, we notice the higher absorption rate due to the presence of RBCs playing the role of solute barriers.

In conclusion, when having high enough Hematocrit (31.3% in this study)

and high enough rigidity of liposome which lead to margination, the presence of RBCs facilitates the vessel wall absorption process. This is mainly due to the impermeability of RBC membrane to the solute. One can speculate that increasing Hematocrit will strengthen the absorption, although further investigations are needed before reaching a definite answer.

5. ATP release from Red Blood Cells under Flow

The study of mechanosensing of solute release can be handled by coupling the boundary conditions with other information such as the membrane shear stress. We apply here our solver to the problem of release of ATP (Adenosine Triphosphate) from RBCs under shear flow. Experimental studies have shown that when RBCs undergo flow originated shear stress, they can release ATP, a universal energy carrier and messenger molecule that plays important role in vessel dilatation Wan et al. (2008); Forsyth et al. (2011). It has been shown in Forsyth et al. (2011) that the amount of ATP release depends on whether RBC undergo tank-treading (TT) or tumbling (TB). In our 2D model a transition from TT to TB can be achieved by increasing the viscosity contrast between the internal and the external fluids Vlahovska et al. (2009). We define the viscosity contrast as $\lambda = \eta_{in}/\eta_{out}$, here η_{in} and η_{out} are the viscosity of internal and external domain of the RBC. A shear flow is generated in a simulation box $[W, L] = [12.5R_0, 25R_0]$ by moving the upper and lower walls with the same speed but opposite direction. The solute (ATP) boundary condition on the upper and the lower walls correspond to zero-flux condition, with periodic

boundary conditions along the flow direction. The RBC is initially located at the center of the shear flow. Experiments have shown that viscosity (as well as the shear rate) contrast is a key parameter to the motion of RBCs under shear flow Fischer et al. (1978); Tsubota and Wada (2010); Fischer and Korzeniewski (2013). For low enough λ (to be specified below), a vesicle (or 2D RBC) tends to exhibit TT motion, whereas for higher λ TB prevails. Two typical values of λ are shown in Fig. 14. We adopt a simplified model of the ATP release, which is a Heaviside step function for shear stress condition (namely, the release takes place only if the local membrane shear stress exceeds a certain value). Thus, the Neumann boundary condition along the membrane for the solute release from RBC towards the external fluid reads

$$D\frac{\partial c}{\partial \mathbf{n}} = \begin{cases} \dot{\gamma}_w/P & \text{if } \sigma > \sigma_0 \\ 0 & \text{if } \sigma \leq \sigma_0 \end{cases}$$

Recall that P is the perimeter of the RBC, $\dot{\gamma}_w$ the wall shear rate, defined in section 4. σ is the shear stress along the membrane, defined as

$$\sigma = \eta_{out}\frac{\partial \mathbf{u_t}}{\partial \mathbf{n}}$$

where $\mathbf{u_t}$ is the fluid velocity along the membrane tangent.

The critical value of the shear stress is set to $\sigma_0 = 0.07Pa$, and is inspired by *in vitro* experiments Forsyth et al. (2011). We use the ATP diffusivity $D_{ATP} = 2.36 \times 10^{-10} m^2/s$, which leads to the Peclet number $Pe = \dot{\gamma}_w R_0^2/D = 1.91$. The ATP concentration field snapshots is shown in Fig. 14 with $\lambda = 1$ (TT) and $\lambda = 8$ (TB). Our results show that qualitatively an increase of viscosity contrast

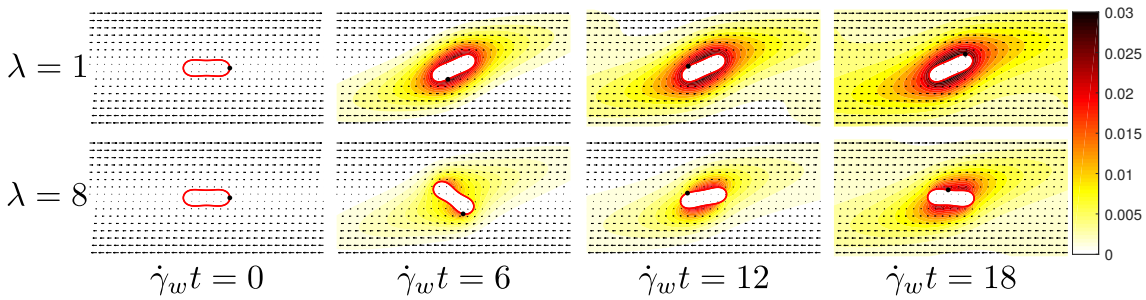

Figure 14: ATP fields under different viscosity contrast values. For $\lambda = 1$, the vesicles undergo tank-treading motion, while for $\lambda = 8$, the tumbling motion prevails. In the tumbling regime the release pattern along the membrane is more inhomogeneous, but the overall released concentration is lesser than in the tank-treading regime ($\lambda = 1$).

reduces the ATP release. In other words, the TB regime triggers less release than the TT one. This finding is consistent with experimental observations Forsyth et al. (2011). Actually the problem is more subtle, since not only the local shear stress matters, but also the cell deformation amplitude. By taking into account both effects, we have been able to reproduce both qualitatively and quantitatively the experimental results. An extensive study is devoted to this question in a different publication Zhang et al. (2018).

6. Conclusion

In this work, we developed a 2D lattice-Boltzmann based advection-diffusion solver for curved moving boundaries for both Dirichlet, Neumann and linear Robbin boundary conditions. In most cases, a second order convergence is achieved. For highly distorted boundaries, a convergence between first and second order is observed. The boundary scheme requires only one neighboring

lattice point with simple strategy, allowing for efficient GPU parallelization.

Since the advection-diffusion solver is designed for generic usage, its implementation for other problems, such as two-sided coupling cases is straightforward. Moreover, the scheme is based on a simple pixelization of curved boundary, with the help of parallel voxelizer, implying that the extension to 3D is also feasible.

We coupled this solver to a well-validated immersed boundary lattice-Boltzmann fluid-vesicle solver and implemented the resulting code for the study of liposome based hydrophilic drug delivery problem. We confirmed that with an assumption of instant absorption on vessel wall, when the liposome margination effect is strong, the presence of red blood cells facilitates the absorption. We have also demonstrated the potential of using this solver for shear stress induced cell-signaling process, and have exemplified it for the problem of ATP release by RBCs under flow.

bf Acknowledgements

C.M. and H.Z. acknowledge financial support from CNES (Centre National d'Etudes Spatiales), the French-German University Programme "Living Fluids" (Grant CFDA-Q1-14), and the China Scholarship Council (CSC).

Appendix A. Asymptotic Analysis of the Bulk Equations and Boundary Conditions

In this appendix, we show on one hand that the lattice-Boltzmann equations are equivalent in the asymptotic limit to the advection-diffusion equation and

on the other hand they allow to derive the boundary conditions (Eq. (13)); see Huang and Yong (2015). Similar procedures were used in Junk et al. (2005); Yoshida and Nagaoka (2010) for other strategy of handling boundary conditions, different from that given by Eq. (13) (which we may view as a modified bounce-back scheme). By using our strategy, we will prove analytically here that this boundary condition enjoys a second order precision. We deal here with the zigzag boundary which is defined to pass through the middle of the mesh segment (dashed line in Fig. 1 (b)). It is this choice that allowed us to reach the second-order precision.

Let us first introduce the diffusive scaling which is based on the idea of finding a suitable pair of scaling size (which is also the numerical mesh size) $(\Delta t, \Delta x)$ that makes the diffusivity in numerical simulation $D^{'}$ (as it was defined in Eq. (9)) close to $O(1)$ in magnitude. This conditions reads

$$D^{'} = \frac{\Delta t}{\Delta x^2} D \sim O(1) \tag{A.1}$$

The following choice of scales satisfies our constraint

$$\begin{aligned} \Delta t = &\quad a\epsilon^2 \\ \Delta x = &\quad \epsilon \end{aligned} \tag{A.2}$$

Here $a = \Delta t/\Delta x^2 = D^{'}/D$ is a constant value representing the ratio between numerical diffusivity $D^{'}$ and physical diffusivity D. The factor ϵ is a small parameter and is often introduced in this way in the context of asymptotic

analysis. Accordingly the scaling of velocity is given by

$$\mathbf{u}^{'} = \frac{\Delta t}{\Delta x}\mathbf{u} = a\epsilon\mathbf{u} \tag{A.3}$$

Our asymptotic analysis below obtained in the limit $\epsilon \to 0$ will show that (i) the Boltzmann equation recovers the advection-diffusion equation, and (ii) the convergence to the advection-diffusion equation is of order $O(\epsilon^2)$ for both the bulk equations and the boundary conditions.

The Boltzmann equation (combining collision and streaming process (equation (5 - 7)) reads, by omitting the reaction term, as

$$g_i(t + a\epsilon^2, \mathbf{x} + \hat{c}_i\epsilon) - g_i = \frac{1}{\tau}\left[w_i c(1 + 3a\mathbf{u}\cdot\hat{c}_i\epsilon) - g_i\right] \tag{A.4}$$

The unspecified argument in g_i is $(t, \mathbf{x})$ and is omitted here, $\hat{c}_i = \mathbf{c}_i/(\Delta x/\Delta t)$ is the normalized unit vector of micro velocities defined in Eq. (4).

We will expand g_i and c in powers of ϵ up to third order. It turns out that the second order provides the leading order contribution for the advection-diffusion problem, whereas the third order is necessary for obtaining the desired precision. The expansion reads

$$\begin{cases} g_i = g_i^{(0)} + \epsilon g_i^{(1)} + \epsilon^2 g_i^{(2)} + \epsilon^3 g_i^{(3)} + O(\epsilon^4) \\ c = c^{(0)} + \epsilon c^{(1)} + \epsilon^2 c^{(2)} + \epsilon^3 c^{(3)} + O(\epsilon^4) \end{cases} \tag{A.5}$$

Expanding Eq. (A.4) in power series of ϵ and ignoring terms of higher order

than ϵ^3 we obtain

$$g_i(t + a\epsilon^2, \mathbf{x} + \hat{c}_i\epsilon) - g_i = \sum_{n=1}^{3} \frac{1}{n!} \left(a\epsilon^2 \frac{\partial}{\partial t} + \epsilon(\hat{c}_i \cdot \nabla) \right)^n g_i + O(\epsilon^4) \tag{A.6}$$

For Eq. (1) we get

$$\sum_{n=0}^{3} \left(c^{(n)} - \sum_{i=0}^{4} g^{(n)} \right) \epsilon^n + O(\epsilon^4) = 0 \tag{A.7}$$

Equating terms of similar order in ϵ in (A.7) provides

$$c^{(n)} = \sum_{i=0}^{4} g_i^{(n)} \tag{A.8}$$

Reporting (A.5) and (A.6) into (A.4) we obtain, by equating terms of the same order, the following hierarchical equations

$$\begin{aligned}
g_i^{(0)} =& w_i c^{(0)} \\
g_i^{(1)} =& w_i c^{(1)} + \frac{1}{2} a\hat{c}_i \cdot \mathbf{u} c^{(0)} - \tau(\hat{c}_i \cdot \nabla) g_i^{(0)} \\
g_i^{(2)} =& w_i c^{(2)} + \frac{1}{2} a\hat{c}_i \cdot \mathbf{u} c^{(1)} - \tau(\hat{c}_i \cdot \nabla) g_i^{(1)} - \tau \left[a\frac{\partial}{\partial t} + \frac{1}{2}(\hat{c}_i \cdot \nabla)^2 \right] g_i^{(0)} \\
g_i^{(3)} =& w_i c^{(3)} + \frac{1}{2} a\hat{c}_i \cdot \mathbf{u} c^{(2)} - \tau(\hat{c}_i \cdot \nabla) g_i^{(2)} - \tau \left[a\frac{\partial}{\partial t} + \frac{1}{2}(\hat{c}_i \cdot \nabla)^2 \right] g_i^{(1)} - \tau \left[a(\hat{c}_i \cdot \nabla)\frac{\partial}{\partial t} + \frac{1}{6}(\hat{c}_i \cdot \nabla)^3 \right] g_i^{(0)}
\end{aligned} \tag{A.9}$$

By summing over i (from 0 to 4) the first equation in (A.9), and using Eq.(A.8) and the fact that the weight factors obey $\sum_{i=0}^{4} w_i = 1$, we find that the resulting equation is automatically satisfied. Performing the same operation with the second equation yields the same conclusion, by using Eq.(A.8) and the first equation in (A.9), and by virtue of the fact that $\sum_{i=0}^{4} \hat{c}_i = 0$, and that

w_i enjoys a symmetry property ($w_1 = w_2$ and $w_3 = w_4$). Performing again the same operation with the third equation, and using the previous orders results leads (after simple algebraic manipulations) to an advection diffusion equation

$$\frac{\partial c^{(0)}}{\partial t} + \mathbf{u} \cdot \nabla c^{(0)} = \nabla \cdot \left[\frac{2\tau - 1}{6a} \nabla c^{(0)} \right] \tag{A.10}$$

Finally, performing the same operation with the last equation yields

$$\frac{\partial c^{(1)}}{\partial t} + \mathbf{u} \cdot \nabla c^{(1)} = \nabla \cdot \left[\frac{2\tau - 1}{6a} \nabla c^{(1)} \right] \tag{A.11}$$

This proves that the lattice Boltzmann scheme (A.4) converges to the advection diffusion equation with an error term $O(\Delta x^2)$. The relation between diffusivity D and relaxation time τ is given by $(2\tau - 1)/(6a) = D$, which also gives $\tau = 3\Delta t/\Delta x^2 D + 1/2$.

Appendix B. Boundary Condition: A Modified Half-Way Bounce-Back Scheme

In this section, we attempt to explain the boundary scheme for the static zigzag boundary, which is given by Eq. (13). This relation has been originally proposed in Ref. Huang and Yong (2015), in which, a second-order convergence is observed in numerical experimentsHuang et al. (2016). We present here a simplified derivation for the particular zigzag boundary which intersects with mesh segments only at middle points (dashed-dotted line in Fig.1 b). Our derivation will prove analytically the second order precision.

A representative point of the discretized boundary is designated as $\mathbf{M}$ in Fig. 2, and $\mathbf{x}$ is a lattice point next to the boundary, and we have the relation

$\mathbf{M} = \mathbf{x} - 1/2\hat{c}_i\Delta x$. A Dirichlet boundary condition is defined as $c(\mathbf{M}) = \alpha_{3,D}^{(mid)}$, whereas a Neumann boundary condition, since the normal direction of the zigzag boundary coincides with $\hat{c}_{\bar{i}}$, can be written as $(\hat{c}_{\bar{i}} \cdot \nabla)c(\mathbf{M}) = \alpha_{3,N}^{(mid)}$. The subscript D and N represents Dirichlet and Neumann respectively. $\bar{i}$ is an index which corresponds to inverse direction of $\hat{c}_i$, that is $\hat{c}_{\bar{i}} = -\hat{c}_i$. However, in the LMB spirit $c(\mathbf{M})$ is not known, since the concentration field is defined at the lattice points only. Therefore we have to express $c(\mathbf{M})$ as a function of its nearest lattice point located at $\mathbf{x}$. Expansion around the lattice point at position $\mathbf{x}$ yields

$$
\begin{aligned}
\alpha_{3,D}^{(mid)} &= c(\mathbf{M}) \\
&= c - \frac{1}{2}\epsilon(\hat{c}_{\bar{i}} \cdot \nabla)c + O(\epsilon^2) \\
&= \left[c^{(0)} - (\frac{1}{2}(\hat{c}_i \cdot \nabla)c^{(0)} - c^{(1)})\right]\epsilon + O(\epsilon^2) \\
\alpha_{3,N}^{(mid)} &= (\hat{c}_{\bar{i}} \cdot \nabla)c(\mathbf{M}) \\
&= -(\hat{c}_i \cdot \nabla)c + \epsilon\frac{1}{2}(\hat{c}_i \cdot \nabla)^2 c + O(\epsilon^2) \\
&= (\hat{c}_i \cdot \nabla)\left[c^{(0)} - \epsilon(\frac{1}{2}(\hat{c}_i \cdot \nabla)c^{(0)} - c^{(1)})\right] + O(\epsilon^2)
\end{aligned}
\tag{B.1}
$$

For brevity, all unspecified arguments on the right hand side are understood to be $(\mathbf{x}, t)$.

The main question now is how to substitute the streaming step (6) at the boundary, in a such a way to respect the above boundary conditions. $g_i(t+\Delta t, \mathbf{x})$ is the unknown incoming distribution function that needs to be determined. Inspired by the traditional bounce back condition (for Navier-stokes equation) we introduce the distribution $g_{\bar{i}}^*(t, \mathbf{x})$, which is the known post-collision distribu-

tion function (defined by Eq. (5)), but defined for opposite micro velocities; the subscript $\bar{i}$ means that the corresponding micro velocity direction is pointing outward (see $\hat{c}_{\bar{i}}$ in Fig. 2). The classical bounce-back boundary condition is given by $g_i(t + \Delta t, \mathbf{x}) = g^*_{\bar{i}}(t, \mathbf{x})$ for zero-flux boundary condition in the pure diffusion problem (the relation is analogous to the non-slip boundary condition in Navier-Stokes LBM). This is quite intuitive, since from time t to $t + 1$ the number of particle crossing the boundary from each side is equal and opposite. The question is how to extend this relation to the present problem.

To deal with this question, we use the same asymptotic expansion in powers if ϵ, as performed in the preceding appendix, for $g^*_{\bar{i}}(t, \mathbf{x})$ and $g_i(t+\Delta t, \mathbf{x})$. With the help of the post-collision and equilibrium distribution function definition (Eq. (5) and (7)) and the asymptotic expansion (equation (A.9)), we find for

$g_{\bar{i}}^*(t,\mathbf{x})$ and $g_i(t+\Delta t,\mathbf{x})$ the following expressions up second order in ϵ

$$
\begin{aligned}
g_{\bar{i}}^*(t,\mathbf{x}) =& g_{\bar{i}}(t,\mathbf{x}) + \frac{1}{\tau}(g_{\bar{i}}^{eq} - g_{\bar{i}}) \\
=& w_i c^{(0)} + \epsilon w_i \left(-(3a\hat{c}_i\cdot\mathbf{u} - (\tau-1)(\hat{c}_i\cdot\nabla))c^{(0)} + c^{(1)}\right) + \\
& \epsilon^2 w_i \left\{(\tau-1)[(\tau-\frac{1}{2})(\hat{c}_i\cdot\nabla)^2 - 3a\hat{c}_i\cdot\mathbf{u}(\hat{c}_i\cdot\nabla) - a\frac{\partial}{\partial t}]c^{(0)} - (3a\hat{c}_i\cdot\mathbf{u} - (\tau-1)(\hat{c}_i\cdot\nabla))c^{(1)} + c^{(2}\right. \\
& O(\epsilon^3) \\
g_i(t+\Delta t,\mathbf{x}) =& g_i(t,\mathbf{x}) + a\epsilon^2\frac{\partial}{\partial t}g_i + O(\epsilon^3) \\
=& w_i c^{(0)} + \epsilon w_i \left((3a\hat{c}_i\cdot\mathbf{u} - (\tau-1)(\hat{c}_i\cdot\nabla))c^{(0)} + c^{(1)}\right) + \\
& \epsilon^2 w_i \left\{[\tau(\tau-\frac{1}{2})(\hat{c}_i\cdot\nabla)^2 - \tau 3a\hat{c}_i\cdot\mathbf{u}(\hat{c}_i\cdot\nabla) - (\tau-1)a\frac{\partial}{\partial t}]c^{(0)} + (3a\hat{c}_i\cdot\mathbf{u} - \tau(\hat{c}_i\cdot\nabla))c^{(1)} + c^{(2)}\right\} \\
& O(\epsilon^3)
\end{aligned}
\tag{B.2}
$$

Here the symmetrical structure of the micro velocities $\hat{c}_i + \hat{c}_{\bar{i}} \equiv 0$ has been exploited. A close inspection of the above equations and the boundary conditions (B.1) allow one to infer the proper writing of the streaming process. Indeed, summation and subtraction of $g_i(t+\Delta t,\mathbf{x})$ and $g_{\bar{i}}^*(t,\mathbf{x})$ provide interesting results if one focuses on zeroth and first order terms only. The results

are given by

$$
\begin{aligned}
\frac{g_{\bar{i}}^{*}(t,\mathbf{x})+g_i(t+\Delta t,\mathbf{x})}{2w_i} &= \left[c^{(0)}-\epsilon(\frac{1}{2}(\hat{c}_i\cdot\nabla)c^{(0)}-c^{(1)})\right]+O(\epsilon^2)\\
\frac{g_{\bar{i}}^{*}(t,\mathbf{x})-g_i(t+\Delta t,\mathbf{x})}{2w_i\epsilon} =& 3a\hat{c}_i\cdot\mathbf{u}\left[c^{(0)}-\epsilon(\frac{1}{2}(\hat{c}_i\cdot\nabla)c^{(0)}-c^{(1)})\right]-\\
&(\tau-\frac{1}{2})(\hat{c}_i\cdot\nabla)\left[c^{(0)}-\epsilon(\frac{1}{2}(\hat{c}_i\cdot\nabla)c^{(0)}-c^{(1)})\right]+O(\epsilon^2)
\end{aligned}
\tag{B.3}
$$

Interestingly, the right hand sides of Eqs. (B.3) are linear combination of the boundary condition (Eq.(B.1)), and in addition they both have the same magnitude regarding the error term $O(\epsilon^2)$. By substituting $\alpha_{3,D}^{(mid)}$ and $\alpha_{3,N}^{(mid)}$ (given by Eq. (B.1)) into Eq.(B.3), the boundary scheme (Eq. (13)) can be straightforwardly extracted. Note that in the special case when $\mathbf{u}\equiv 0$ and $\alpha_{3,N}^{(mid)}\equiv 0$, the boundary scheme will coincide with the classical bounce-back one. An important point is worth of mention. The choice of the zigzag boundary passing precisely at the middle of the lattice segments is not innocuous. Had we chosen another definition, then the precision would have degraded down to lower order, namely $O(\epsilon)$ instead of enjoying $O(\epsilon^2)$ precision.

Akbarzadeh A, Rezaei-Sadabady R, Davaran S, Joo SW, Zarghami N, Hanifehpour Y, Samiei M, Kouhi M, Nejati-Koshki K. Liposome: classification, preparation, and applications. Nanoscale Res Lett 2013;8(1):102.

Allen TM, Cullis PR. Liposomal drug delivery systems: from concept to clinical applications. Adv Drug Deliv Rev 2013;65(1):36–48.

Ando J, Yamamoto K. Flow detection and calcium signalling in vascular endothelial cells. Cardiovasc Res 2013;99(2):260–8.

Betz T, Lenz M, Joanny JF, Sykes C. Atp-dependent mechanics of red blood cells. Proceedings of the National Academy of Sciences 2009;106(36):15320–5.

Chen KY, Lai MC. A conservative scheme for solving coupled surface-bulk convection–diffusion equations with an application to interfacial flows with soluble surfactant. J Comput Phys 2014;257:1–18.

Chen Q, Zhang X, Zhang J. Improved treatments for general boundary conditions in the lattice boltzmann method for convection-diffusion and heat transfer processes. Phys Rev E 2013a;88(3):033304.

Chen Q, Zhang X, Zhang J. Improved treatments for general boundary conditions in the lattice boltzmann method for convection-diffusion and heat transfer processes. Phys Rev E 2013b;88(3):033304.

Chen S, Doolen GD. Lattice boltzmann method for fluid flows. Annu Rev Fluid Mech 1998;30(1):329–64.

Davies PF. Flow-mediated endothelial mechanotransduction. Physiol Rev 1995;75(3):519–60.

Fakhari A, Mitchell T, Leonardi C, Bolster D. Improved locality of the phase-field lattice-boltzmann model for immiscible fluids at high density ratios. Phys Rev E 2017;96:053301. URL: `https://link.aps.org/doi/10.1103/PhysRevE.96.053301`. doi:`10.1103/PhysRevE.96.053301`.

Feng ZG, Michaelides EE. The immersed boundary-lattice boltzmann method for solving fluid–particles interaction problems. Journal of Computational Physics 2004;195(2):602–28.

Fischer TM, Korzeniewski R. Threshold shear stress for the transition between tumbling and tank-treading of red blood cells in shear flow: dependence on the viscosity of the suspending medium. J Fluid Mech 2013;736:351365. doi:10.1017/jfm.2013.496.

Fischer TM, Stohr-Lissen M, Schmid-Schonbein H. The red cell as a fluid droplet: tank tread-like motion of the human erythrocyte membrane in shear flow. Science 1978;202(4370):894–6.

Forsyth AM, Wan J, Owrutsky PD, Abkarian M, Stone HA. Multiscale approach to link red blood cell dynamics, shear viscosity, and atp release. Proc Natl Acad Sci USA 2011;108(27):10986–91. doi:10.1073/pnas.1101315108.

Gebäck T, Heintz A. A lattice boltzmann method for the advection-diffusion equation with neumann boundary conditions. Comm Comput Phys 2014;15(2):487–505.

Gekle S. Strongly accelerated margination of active particles in blood flow. Biophys J 2016;110(2):514–20.

Gekle S. Dispersion of solute released from a sphere flowing in a microchannel. J Fluid Mech 2017;819:104–20.

Guckenberger A, Gekle S. A boundary integral method with volume-changing

objects for ultrasound-triggered margination of microbubbles. J Fluid Mech 2018;836:952–97.

He X, Luo LS. Theory of the lattice boltzmann method: From the boltzmann equation to the lattice boltzmann equation. Phys Rev E 1997;56(6):6811.

Hu WF, Lai MC, Misbah C. A coupled immersed boundary and immersed interface method for interfacial flows with soluble surfactant. Comput Fluids 2018;168:201–15.

Huang H, Sugiyama K, Takagi S. An immersed boundary method for restricted diffusion with permeable interfaces. J Comput Phys 2009;228(15):5317–22.

Huang J, Hu Z, Yong WA. Second-order curved boundary treatments of the lattice boltzmann method for convection–diffusion equations. J Comput Phys 2016;310:26–44.

Huang J, Yong WA. Boundary conditions of the lattice boltzmann method for convection–diffusion equations. J Comput Phys 2015;300:70–91.

Jafarnejad M, Cromer W, Kaunas R, Zhang S, Zawieja D, Moore Jr J. Measurement of shear stress-mediated intracellular calcium dynamics in human dermal lymphatic endothelial cells. Am J Physiol Heart Circ Physiol 2015;308(7):H697–706.

Junk M, Klar A, Luo LS. Asymptotic analysis of the lattice boltzmann equation. J Comput Phys 2005;210(2):676–704.

Kabacaoğlu G, Quaife B, Biros G. Quantification of mixing in vesicle suspensions using numerical simulations in two dimensions. Phys Fluids 2017;29(2):021901.

Kaoui B. Computer simulations of drug release from a liposome into the bloodstream. Eur Phys J E 2018;41(2):20.

Kaoui B, Ristow GH, Cantat I, Misbah C, Zimmermann W. Lateral migration of a two-dimensional vesicle in unbounded poiseuille flow. Phys Rev E 2008;77:021903. URL: https://link.aps.org/doi/10.1103/PhysRevE.77.021903. doi:10.1103/PhysRevE.77.021903.

Kaoui B, Tahiri N, Biben T, Ez-Zahraouy H, Benyoussef A, Biros G, Misbah C. Complexity of vesicle microcirculation. Phys Rev E 2011;84:041906.

Krüger T. Effect of tube diameter and capillary number on platelet margination and near-wall dynamics. Rheol Acta 2016;55(6):511–26.

Krüger T, Frijters S, Günther F, Kaoui B, Harting J. Numerical simulations of complex fluid-fluid interface dynamics. The European Physical Journal Special Topics 2013;222:177–98.

Krüger T, Kusumaatmaja H, Kuzmin A, Shardt O, Silva G, Viggen EM. The Lattice Boltzmann Method. Springer, 2017.

Kumar A, Graham MD. Mechanism of margination in confined flows of blood and other multicomponent suspensions. Phys Rev Lett 2012;109(10):108102.

Lallemand P, Luo LS. Lattice boltzmann method for moving boundaries. J Comput Phys 2003;184(2):406–21.

Lee P, Griffith BE, Peskin CS. The immersed boundary method for advection–electrodiffusion with implicit timestepping and local mesh refinement. J Comput Phys 2010;229(13):5208–27.

Li L, Mei R, Klausner JF. Boundary conditions for thermal lattice boltzmann equation method. J Comput Phys 2013;237:366–95.

Li L, Mei R, Klausner JF. Lattice boltzmann models for the convection-diffusion equation: D2q5 vs d2q9. International Journal of Heat and Mass Transfer 2017;108:41–62.

Liu Z, Zhu Y, Rao R, Clausen J, Aidun C. Nanoparticle transport in cellular blood flow. Computers and Fluids 2018;172:609–20.

Markl M, Körner C. Free surface neumann boundary condition for the advection–diffusion lattice boltzmann method. J Comput Phys 2015;301:230–46.

Mohamad AA. Lattice Boltzmann method: fundamentals and engineering applications with computer codes. Springer Science & Business Media, 2011.

Müller K, Fedosov DA, Gompper G. Understanding particle margination in blood flow–a step toward optimized drug delivery systems. Med Eng Phys 2016;38(1):2–10.

Needham D, Anyarambhatla G, Kong G, Dewhirst MW. A new temperature-sensitive liposome for use with mild hyperthermia: characterization and testing in a human tumor xenograft model. Cancer Res 2000;60(5):1197–201.

Novak IL, Slepchenko BM. A conservative algorithm for parabolic problems in domains with moving boundaries. J Comput Phys 2014;270:203–13.

Peskin CS. The immersed boundary method. Acta Numer 2002;11:479–517.

Sercombe L, Veerati T, Moheimani F, Wu SY, Sood AK, Hua S. Advances and challenges of liposome assisted drug delivery. Front Pharmacol 2015;6:286.

Shen Z, Farutin A, Thiébaud M, Misbah C. Interaction and rheology of vesicle suspensions in confined shear flow. Phys Rev Fluids 2017;2(10):103101.

Succi S. The lattice Boltzmann equation: for fluid dynamics and beyond. Oxford university press, 2001.

Suga S. Numerical schemes obtained from lattice boltzmann equations for advection diffusion equations. International Journal of Modern Physics C 2006;17(11):1563–77.

Tsubota Ki, Wada S. Effect of the natural state of an elastic cellular membrane on tank-treading and tumbling motions of a single red blood cell. Phys Rev E 2010;81(1):011910.

Vlahovska PM, Podgorski T, Misbah C. Vesicles and red blood cells: from individual dynamics to rheology. CR Physique 2009;10(1):775.

Wan J, Ristenpart WD, Stone HA. Dynamics of shear-induced atp release from red blood cells. Proc Natl Acad Sci USA 2008;105(43):16432–7.

Yamamoto K, Korenaga R, Kamiya A, Ando J. Fluid shear stress activates ca2+ influx into human endothelial cells via p2x4 purinoceptors. Circ Res 2000;87(5):385–91.

Yang X, Zhang X, Li Z, He GW. A smoothing technique for discrete delta functions with application to immersed boundary method in moving boundary simulations. J Comput Phys 2009;228(20):7821–36.

Yin X, Le G, Zhang J. Mass and momentum transfer across solid-fluid boundaries in the lattice-boltzmann method. Phys Rev E 2012;86(2):026701.

Yoshida H, Nagaoka M. Multiple-relaxation-time lattice boltzmann model for the convection and anisotropic diffusion equation. J Comput Phys 2010;229(20):7774–95.

Zawieja D. Lymphatic biology and the microcirculation: past, present and future. Microcirculation 2005;12(1):141–50.

Zhang H, Shen Z, Hogan B, Barakat AI, Misbah C. Atp release by red blood cells under flow: Model and simulations. Biophysical journal 2018;115:2218–29.

Zhang T, Shi B, Guo Z, Chai Z, Lu J. General bounce-back scheme for concentration boundary condition in the lattice-boltzmann method. Phys Rev E 2012;85(1):016701.

Zhao H, Shaqfeh ES, Narsimhan V. Shear-induced particle migration and margination in a cellular suspension. Phys Fluids 2012;24(1):011902.

Zou Q, He X. On pressure and velocity boundary conditions for the lattice boltzmann bgk model. Phys Fluids 1997;9(6):1591–8.

Zu YQ, He S. Phase-field-based lattice boltzmann model for incompressible binary fluid systems with density and viscosity contrasts. Phys Rev E 2013;87:043301. URL: https://link.aps.org/doi/10.1103/PhysRevE.87.043301. doi:10.1103/PhysRevE.87.043301.